

# Formation Mechanism of Carbogenic Nanoparticles with Dual Photoluminescence Emission

Marta J. Krysmann,<sup>†</sup> Antonios Kelarakis,<sup>†</sup> Panagiotis Dallas, and Emmanuel P. Giannelis\*

Department of Materials Science and Engineering, Cornell University, Ithaca, New York 14853, United States

**S** Supporting Information

**ABSTRACT:** We present a systematic investigation of the formation mechanism of carbogenic nanoparticles (CNPs), otherwise referred to as C-dots, by following the pyrolysis of citric acid (CA)–ethanolamine (EA) precursor at different temperatures. Pyrolysis at 180 °C leads to a CNP molecular precursor with a strongly intense photoluminescence (PL) spectrum and high quantum yield formed by dehydration of CA–EA. At higher temperatures (230 °C) a carbogenic core starts forming and the PL is due to the presence of both molecular fluorophores and the carbogenic core. CNPs that exhibit mostly or exclusively PL arising from carbogenic cores are obtained at even higher temperatures (300 and 400 °C, respectively). Since the molecular fluorophores predominate at low pyrolysis temperatures while the carbogenic core starts forming at higher temperatures, the PL behavior of CNPs strongly depends on the conditions used for their synthesis.

Photoluminescent compounds are widely used in everyday life as well as in highly specialized applications such as optical analysis, photonics, chemical and biological sensing, molecular tracing, and cellular imaging.<sup>1,2</sup> For the most demanding applications, the fluorescent materials should exhibit structural and photochemical stability in aggressive environments while showing high absorption coefficient and quantum yield ( $\Phi$ ) with minimal toxicity. To meet these requirements, the library of available fluorescent materials (conventional dyes, polymers, or proteins) has been expanded to include colloidal semiconductor nanocrystals (so-called quantum dots),<sup>3</sup> lanthanide chelates,<sup>4</sup> core–shell silica nanoparticles (NPs),<sup>5</sup> and carbogenic nanoparticles (CNPs, known also as C-dots).<sup>6–20</sup> By virtue of their biocompatibility, low toxicity, and ease of preparation, CNPs are environmentally benign alternatives to quantum dots comprised of heavy metals.<sup>7,8</sup> CNPs are often obtained by fragmentation/fractionation of suitable carbon sources followed by surface passivation.<sup>9–11</sup> Alternatively, they can be prepared by bottom-up strategies utilizing molecular precursors and simple techniques such as combustion, thermal, or microwave treatments.<sup>12–20</sup> Our group has reported a one-step thermal decomposition of citric acid (CA)-based molecular precursors to synthesize surface-passivated CNPs with hydrophilic or hydrophobic surface groups.<sup>14,15</sup>

In this report, we present a systematic study of the formation mechanism of CNPs from molecular precursors and demon-

strate that their photoluminescence (PL) can arise from two different sources. Following pyrolytic decomposition of CA and ethanolamine (EA) (1:3 molar ratio), we isolate three distinct photoluminescent species (which correspond to three different stages of the pyrolysis) and show that each exhibits a distinct emission behavior. At low temperatures pyrolysis leads to a CNP precursor whose intense PL is due to organic fluorophores. As the pyrolysis proceeds to higher temperatures, the CNP precursor is gradually consumed in favor of the CNPs. At high pyrolysis temperatures, CNPs are formed and their carbogenic cores are the main source of their PL, with the PL intensity and  $\Phi$  much diminished. At intermediate temperatures the PL can be resolved into two components, one stemming directly from their intrinsic carbogenic core and the other from the presence of amide-containing fluorophores. The results presented here rationalize the disparate and often confusing behavior reported in terms of PL intensity and  $\Phi$ . They also provide a straightforward strategy to fine-tune the PL properties of CNPs and optimize them for different applications.

The synthetic approach follows the controlled pyrolysis of CA and EA at different temperatures (above the melting point of CA,  $T_m = 153$  °C) in the absence of solvent. After pyrolysis at 180 °C for 30 min, no NPs are detectable by either DLS or TEM. Instead, a fluid that is bright yellow, highly photoluminescent, and readily soluble in water is obtained, referred to as CNP180. The UV–vis spectrum of the sample in water is shown in Supporting Information (SI) Figure 1a. The <sup>15</sup>N NMR<sup>21</sup> (SI Figure 2), XPS<sup>22</sup> (SI Figure 3), and FTIR spectra (SI Figure 4c) suggest the presence of amide functional groups in the product formed by a simple intermolecular condensation reaction accompanied by loss of water molecules (Scheme 1).<sup>23–25</sup>

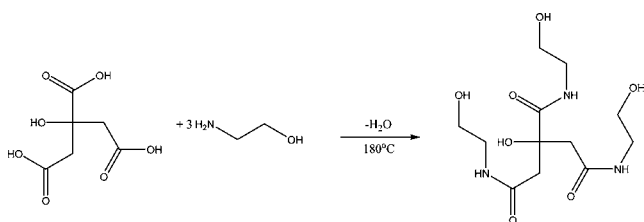
To further elucidate the molecular character of the product(s) obtained after pyrolysis at 180 °C, the fluid was fractionated by flash chromatography over silica gel (70–230 mesh) using DCM/methanol (6:4 v:v) as the mobile phase. The highly fluorescent fraction (referred to as PL-CNP180) was characterized by <sup>1</sup>H and <sup>13</sup>C NMR, FTIR, XPS, ESI-MS, and MS/MS.

The FTIR spectrum of PL-CNP180 (SI Figure 4d) confirms the presence of amide functional groups, as evidenced by their vibrational fingerprints centered at 1550 (N–H in-plane bending), 1636 (C=O stretching of the amide bond), and 3300 cm<sup>-1</sup> (N–H stretching). The XPS spectra (SI Figure 5)

Received: May 21, 2011

Published: December 25, 2011

## Scheme 1. Reaction Scheme of EA and CA toward the Formation of PL-CNP180



also confirm the presence of amide groups.<sup>22</sup> Specifically, amide carbonyl groups (C 1s at 288.2 eV), amide nitrogen (N 1s at 401 eV), carbonyl oxygen (O 1s 533.5 eV), and aliphatic carbons (C 1s at 286.3 eV) can be seen in the spectra.

The <sup>1</sup>H and <sup>13</sup>C NMR spectra of the PL-CNP180 are shown in SI Figure 6. With respect to <sup>1</sup>H NMR, the upfield (2.6 ppm) and downfield (2.8 ppm) doublet peaks can be attributed to methylene protons of the CA, the triplet at 3.3 ppm to the protons of the hydroxyethyl group adjacent to the amide bond, and the triplet at 3.7 ppm to the protons on the hydroxyethyl group next to the hydroxyl group. With respect to <sup>13</sup>C NMR, the peak at 171.7 ppm is due to carbons in the amide bonds, the peaks at 74.9 and 59.8 ppm to carbons adjacent to hydroxyl groups, the peak at 43.6 ppm to methylene carbons, and the peak at 41.2 ppm to carbon near the amide bond.

More importantly, the ESI-MS spectrum (SI Figure 7) suggests a native molecule (M) with  $m/z = 321$ , which is identical to the product in Scheme 1. The assignment is based on the presence of M<sup>-</sup> at  $m/z = 320$  (negative spectra) and the detection of the adduct ions with  $m/z = 322$  (M-H<sup>+</sup>), 344 (M-Na<sup>+</sup>), 360 (M-K<sup>+</sup>), and 665 (2M-Na<sup>+</sup>) (positive spectra). (Our analysis was further supported by MS/MS data listed in SI Figure 7.)

Together, the experimental evidence unambiguously suggests that pyrolysis at 180 °C follows the reaction shown in Scheme 1 and results in a molecular precursor containing amide groups. The strong PL of model amides (maximum at  $\lambda_{em} = 455 \pm 15$  nm) has been assigned to a direct singlet-to-triplet transition.<sup>26</sup>

To further confirm the mechanism, an alternative synthesis approach (SI Figure 8a) was also used. EA and CA were dissolved in water and kept in an ice bath to allow the formation of tris(2-hydroxyethyl)ammonium citrate salt (SI Salt Synthesis). Upon heating, the citrate salt undergoes dehydration at 140 °C under vacuum to form an amide that is identical to the PL-CNP180 molecule (SI Figure 8b,c). Given that the photophysical properties of PL-CNP180 closely resemble those of the CNP180, we focus below on the PL behavior of the latter system (for comparison the PL spectra of PL-CNP180 are shown in SI Figure 9, while its UV-vis spectrum is shown in SI Figure 1). Particularly, the excitation of an aqueous solution of the CNP180 between 200 and 400 nm shows a single, excitation-independent PL (Figure 1a) that is characterized by a remarkably high  $\Phi \approx 50\%$ . The emission band centers at  $\lambda_{em} = 455$  nm and shows maximum intensity at  $\lambda_{ex} = 375$  nm.

The emission intensity exhibits a plateau within the pH range 4–12, but decreases abruptly at lower pH (Figure 2a). The reversible effects of pH can be understood in terms of extensive protonation–deprotonation of the amide group given that the deprotonated amide groups have much higher electron-donating efficiency. Finally, we note that excitation above  $\lambda_{ex} > 400$  nm fails to induce any measurable emission (Figure 1a).

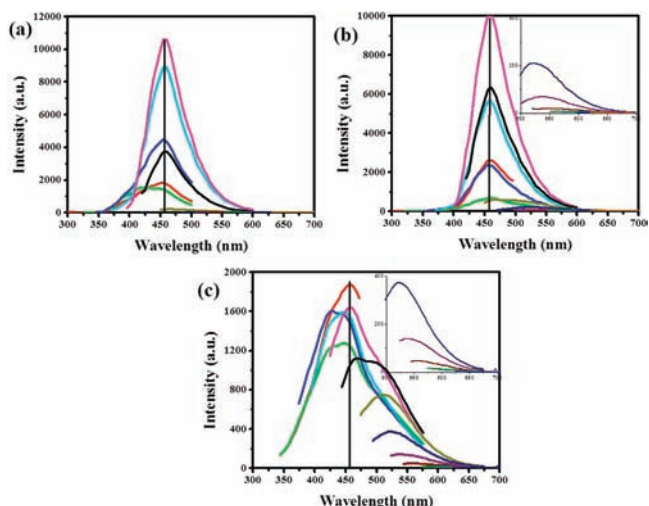


**Figure 1.** PL spectra of aqueous dispersions of (a) CNP180, (b) CNP230, and (c) CNP300. The sample concentration was 0.1 mg/mL. The excitation wavelength was varied from 275 to 600 nm with a fixed increment of 25 nm. Colors correspond to different excitation wavelengths: red, green, blue, cyan, magenta, black, dark yellow, navy, purple, wine, dark cyan, royal, and orange correspond to 275, 300, 325, 350, 375, 400, 425, 450, 475, 500, 525, 550, 575, and 600 nm.

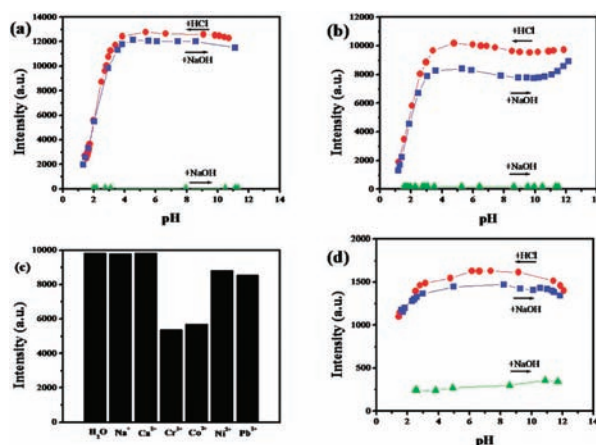


**Figure 2.** pH dependence of the maximum PL intensity of aqueous dispersions of (a) CNP180, (b) CNP230, and (d) CNP300. Spectra recorded at  $\lambda_{ex} = 375$  nm (red circles, decreasing pH) and (blue squares, increasing pH),  $\lambda_{ex} = 450$  nm (green triangles). (c) Maximum PL intensity of aqueous dispersions of CNP230 in the presence of various metal ions ( $\lambda_{ex} = 375$  nm).

Pyrolysis at higher temperatures (e.g., at 230 °C for 30 min) produces spherical NPs (abbreviated as CNP230), and the sample appears to be light brown. As described in the experimental details in the SI, an essential step of our protocol is the extensive purification of CNP230 through prolonged dialysis to eliminate the presence of the free CNP180. Despite the simplicity and the template-free nature of the preparation method, CNP230 shows spherical symmetry and relatively narrow size distribution, with an average diameter 19 nm (Figure 3a). Buildup of NPs is attributed to extensive cross-linking reactions and formation of interchain imide bonds, as revealed by the band centered at 1776  $\text{cm}^{-1}$  (stretching C=O of the imide group) in the FTIR spectrum (SI Figure 4e). Formation of imide derivatives during pyrolysis has been previously reported.<sup>27</sup> The CNP230 is easily dispersible in

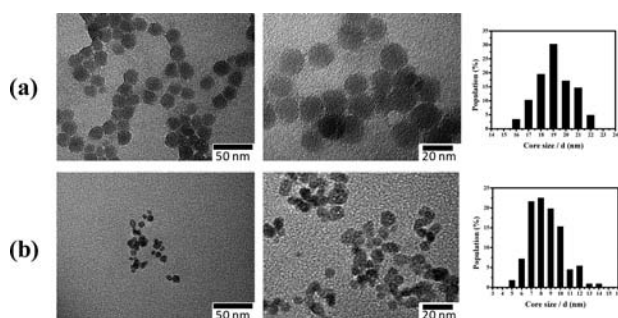


**Figure 3.** TEM images and size histograms (each plotted on the basis of 150 fields) of (a) CNP230 and (b) CNP300.

water and other solvents (e.g., DMSO, DMF, ACN, methanol), confirming the high content of surface polar organic groups. Elemental analysis indicated an increased stoichiometric amount of carbon in CNP230 with an associated decrease in hydrogen (44.85% C, 5.75% H, 10.85% N) compared to CNP180 (41% C, 7.8% H, 11.7% N). From the TEM images, the absence of multiple nuclei embedded within individual particles suggests that pyrolysis at 230 °C leads to single carbogenic domains (cores) with surface organic groups that impart dispersibility.

The luminescence spectra of CNP230 in water between  $200 < \lambda_{\text{ex}} < 400$  nm show a maximum at 455 nm with the strongest intensity recorded for  $\lambda_{\text{ex}} = 375$  nm (Figure 1b). In that sense, the emission mode of CNP230 closely resembles that of the precursor. However, the  $\Phi$  for CNP230 is only  $\sim 15\%$ . This value is significantly lower compared to CNP180 ( $\Phi \approx 50\%$ ) and suggests that a large amount of the fluorophores are used as the building blocks of the carbogenic domains. On the other hand, excitation with longer wavelengths ( $\lambda_{\text{ex}} > 400$  nm) induces an excitation-dependent emission, given that as  $\lambda_{\text{ex}}$  increases the emission spectra are systematically displaced toward longer wavelengths and the intensity decreases (Figure 1b inset). The dependence of emission wavelength and intensity on  $\lambda_{\text{ex}}$  has been identified as a generic feature of various types of CNPs.<sup>6</sup>

As shown in Figure 2b, the emission maximum at  $\lambda_{\text{ex}} = 375$  nm is relatively stable within the pH range 4–12, but falls dramatically below pH < 4. The maximum intensity ( $\lambda_{\text{ex}} = 450$  nm) of the excitation-wavelength-dependent emission is essentially unchanged over a broad pH range (Figure 2b). The PL emission is significantly reduced in the presence of 3d metal ions Cr(III) and Co(II) (but not in the presence of other metals shown in Figure 2c), due to a selective metal–fluorophore complexation.<sup>28</sup> These preliminary results suggest that sensor platforms based on CNPs can in principle respond to complex environments, serving for example as probes for the detection of analytically important metals that is of vital importance for environmental monitoring and wastewater management.<sup>29</sup>

Further pyrolysis (at 300 °C for 1 h) results in much more darkening of the sample and the formation of CNPs (abbreviated as CNP300) with an average diameter of 8 nm (Figure 3b), consistent with earlier reports of CNPs with an average diameter of 4–10 nm by various pyrolytic routes.<sup>11–15</sup> (Direct heating of CNP180 at 300 °C yields similar results.) The significantly smaller size of the NPs (compared to  $19 \pm 1$  nm found for CNP230) is consistent with major chemical changes. TGA-MS experiments indicate that during pyrolysis at 300 °C a massive amount of CO<sub>2</sub> escapes from the system that

accounts for the significant shrinkage of CNPs. Elemental analysis (50.5% C, 3.7% H, 13.1% N) indicated an increased amount of carbon with a concomitant decrease in hydrogen compared to CNP230, suggesting that CNP230 underwent further carbonization. In addition, thermogravimetric analysis (TGA) measurements (SI Figure 10) indicate a lower organic content compared to CNP230. Nevertheless, the NPs are well dispersed in water, suggesting the presence of a number of functional groups on their surface. The FTIR spectra (SI Figure 4f) confirm the presence of a certain (although considerably reduced) amount of amide and imide groups that remain stable even after such a high-temperature treatment.

The Raman spectrum of CNP300 is dominated by two peaks centered at approximately 1355 and 1595 cm<sup>-1</sup> that can be identified as the D and G bands of the amorphous carbon, respectively (SI Figure 11a). (For CNP230 strong PL radiation masks the Raman spectra.) The G peak arises from the E<sub>2g</sub> vibration mode of the sp<sup>2</sup> bonded carbon, while the D peak is considered the signature of the disorder in the graphite lattice, since it is assigned to the A<sub>1g</sub> (zone-edge) breathing vibration phonon that is activated only in the presence of a neighboring sp<sup>3</sup> defect.<sup>30,31</sup>

Isolated sp<sup>2</sup> domains dispersed within a sp<sup>3</sup> matrix can function as PL centers, an effect that is governed by the  $\pi$  states of sp<sup>2</sup> sites.<sup>32</sup> In particular, the PL behavior of amorphous/disordered graphites containing a mixture of sp<sup>2</sup> and sp<sup>3</sup> carbons has been attributed to the photogeneration of electron–hole pairs that can induce radiative recombination of the trap carriers localized within small sp<sup>2</sup> carbon clusters, which are surrounded by sp<sup>3</sup> defects, a mechanism that can remain active in the presence of heteroatoms.<sup>32,33</sup> Evidently, this photophysical mechanism can function in parallel with other emission modes (induced from the organic fluorophores).

The dual emissive mode of the CNP300 in water is clearly seen in Figure 1c that displays a series of emission spectra recorded at various excitation wavelengths,  $\lambda_{\text{ex}}$ . Between  $200 < \lambda_{\text{ex}} < 400$  nm, the PL band is composed of two largely overlapping peaks, one that has a maximum at a fixed position  $\lambda_{\text{em}} = 455$  nm with  $\Phi \approx 4\%$  (for which the stronger signal is recorded for  $\lambda_{\text{ex}} = 375$  nm) and another that monotonically red-shifts with increasing  $\lambda_{\text{ex}}$ . The latter dominates the spectra at  $\lambda_{\text{ex}} > 400$  nm. As in the case of CNP230, we attribute the excitation-independent emission to the presence of organic fluorophores and the excitation-dependent emission to the carbogenic cores. Due to the limited organic content of CNP300, the  $\Phi$  and the pH dependence of the organo-fluorophore emission are much suppressed compared to CNP230 (Figure 2d). In addition, the emission due to the carbogenic domains remains virtually unchanged with pH (Figure 2d).

Further pyrolysis (at 400 °C for 1 h) gives rise to clustering and the formation of larger and nonuniform carbogenic particles (abbreviated as CNP400) with diameters in the order of a few hundred nanometers, presumably due to aggregation (SI Figure 12). The FTIR spectrum (SI Figure 2g) indicates the absence of any functional groups, while elemental analysis suggests almost zero nitrogen content. The Raman spectrum of CNP400 shows both G and D peaks (SI Figure 11b). The dispersibility of CNP400 in water is relatively limited. Nevertheless, the dispersion exhibits excitation-dependent emission, although the intensity is low (SI Figure 13a). The dispersibility of the particles is significantly enhanced after

treatment with HNO<sub>3</sub> that allows surface oxidation of the fluorophore-free CNP400 (abbreviated as ox-CNP400). The ox-CNP400 exhibit excitation-dependent emission PL within the range 375 <  $\lambda_{\text{ex}}$  < 600 nm (SI Figure 13b), in line with the observations presented above (for  $\lambda_{\text{ex}}$  < 375 nm the PL intensity is too low to be measured).

Figure 4 summarizes our findings. The schematic correlates the PL intensity (and  $\Phi$ ) of the species obtained during

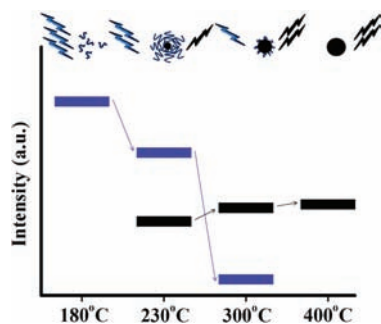


**Figure 4.** Schematic representation of the emission characteristics of three photoactive species produced from the thermal treatment of mixture of CA and EA. During pyrolysis, the organic fluorophores (blue groups) are consumed for the buildup of the carbogenic core (black sphere) so that the PL component that corresponds to the carbogenic core (black bars) increases at the expenses of the component that arises from the organic fluorophores (blue bars).

different stages of pyrolysis. At first a CNP precursor with a strongly intense PL spectrum and high  $\Phi$  is formed. The PL spectrum is mostly due to amide-containing fluorophores (blue groups). As the pyrolysis proceeds to higher temperatures a carbogenic core (black spheres) is formed at the expense of the molecular fluorophores. Eventually, CNPs that exhibit mostly or exclusively PL arising from carbogenic cores are obtained. The well-established quenching efficiency of graphitic particles with respect to the emission of neighboring or absorbed dyes<sup>34</sup> might account to some extent for the suppressed emission of the organic fluorophores observed for CNP230 and CNP300.

## ■ ASSOCIATED CONTENT

### ● Supporting Information

Detailed experimental procedures and characterization by <sup>14</sup>N, <sup>1</sup>H, and <sup>13</sup>C NMR, XPS, UV-vis, FTIR, and Raman spectra, ESI-MS, and TGA. This material is available free of charge via the Internet at <http://pubs.acs.org>.

## ■ AUTHOR INFORMATION

### Corresponding Author

epg2@cornell.edu

### Author Contributions

<sup>†</sup>These authors contributed equally to this work.

## ■ ACKNOWLEDGMENTS

This publication is based on work supported in part by Award No. KUS-C1-018-02 made by King Abdullah University of Science and Technology. It is also based on work supported in part by Torrey Pines and the Energy Materials Center at Cornell, an Energy Frontier Research Center funded by the U.S. Department of Energy, Office of Science, Office of Basic Energy Sciences, under Award No. DE-SC0001086. M.J.K. and

A.K. dedicate this Communication to Prof. Colin Booth (Manchester University) on the occasion of his 80th birthday.

## ■ REFERENCES

- (1) Mattoussi, H.; Mauro, M.; Goldman, E. R.; Anderson, G. P.; Sundar, V. C.; Mikulec, F. V.; Bawendi, M. G. *J. Am. Chem. Soc.* **2000**, *122*, 12142.
- (2) Wu, B. Y.; Wang, H. F.; Chen, J. T.; Yan, X. P. *J. Am. Chem. Soc.* **2011**, *133*, 686.
- (3) Qu, L.; Peng, X. *J. Am. Chem. Soc.* **2002**, *124*, 2049.
- (4) Li, M.; Selvin, P. R. *J. Am. Chem. Soc.* **1995**, *117*, 8132.
- (5) Burns, A.; Ow, H.; Wiesner, U. *Chem. Soc.* **2006**, *35*, 1028.
- (6) Baker, S. N.; Baker, G. A. *Angew. Chem., Int. Ed.* **2010**, *49*, 6726.
- (7) Yang, S.-T.; Cao, L.; Luo, P. G.; Lu, F.; Wang, X.; Wang, H.; Meziani, M. J.; Liu, Y.; Qi, G.; Sun, Y. P. *J. Am. Chem. Soc.* **2009**, *131*, 11308.
- (8) Yang, S.-T.; Wang, X.; Wang, H.; Lu, F.; Luo, P. G.; Cao, L.; Meziani, M. J.; Liu, J.-H.; Liu, Y.; Chen, M.; Huang, Y.; Sun, Y.-P. *J. Phys. Chem. C* **2009**, 18110.
- (9) Sun, Y. P.; Zhou, B.; Lin, Y.; Wang, W.; Fernando, K. A. S.; Pathak, P.; Meziani, M. J.; Harruff, B. A.; Wang, X.; Wang, H.; Luo, P. G.; Yang, H.; Kose, M. E.; Chen, B.; Veca, L. M.; Xie, S. Y. *J. Am. Chem. Soc.* **2006**, *128*, 7756.
- (10) Zhou, J.; Booker, C.; Li, R.; Zhou, X.; Sham, T. K.; Sun, X.; Ding, Z. *J. Am. Chem. Soc.* **2007**, *129*, 744.
- (11) Cao, L.; Wang, X.; Meziani, M. J.; Lu, F.; Wang, H.; Luo, P. G.; Lin, Y.; Harruff, B. A.; Veca, L. M.; Murray, D.; Xie, S. Y.; Sun, Y. P. *J. Am. Chem. Soc.* **2007**, *129*, 11318.
- (12) Pan, D.; Zhang, J.; Li, Z.; Wu, C.; Yan, X.; Wu, M. *Chem. Commun.* **2010**, *46*, 3681.
- (13) Ray, S. C.; Saha, A.; Jana, N. R.; Sarkar, R. *J. Phys. Chem. C* **2009**, *113*, 18549.
- (14) Bourlinos, A. B.; Stassinopoulos, A.; Anglos, D.; Zboril, R.; Karakassides, M.; Giannelis, E. P. *Small* **2008**, *4*, 455.
- (15) Bourlinos, A. B.; Stassinopoulos, A.; Anglos, D.; Zboril, R.; Georgakilas, V.; Giannelis, E. P. *Chem. Mater.* **2008**, *20*, 4539.
- (16) Wang, F.; Pang, S.; Wang, L.; Li, Q.; Kreiter, M.; Liu, C.-Y. *Chem. Mater.* **2010**, *22*, 4528.
- (17) Peng, H.; Travas-Sejdic, J. *Chem. Mater.* **2009**, *21*, 5563.
- (18) Zhu, H.; Wang, X.; Li, Y.; Wang, Z.; Yanga, F.; Yang, X. *Chem. Commun.* **2009**, 5118.
- (19) Liu, R.; Wu, D.; Liu, S.; Koynov, K.; Knoll, W.; Li, Q. *Angew. Chem., Int. Ed.* **2009**, *48*, 4598.
- (20) Liu, H.; Ye, T.; Mao, C. *Angew. Chem., Int. Ed.* **2007**, *46*, 6473.
- (21) Schwarzwinger, S.; Kroon, G. J. A.; Foss, T. R.; Chung, J.; Wright, P. E.; Dyson, H. J. *J. Am. Chem. Soc.* **2001**, *123*, 2970.
- (22) Buchwalter, L. P. *J. Vac. Sci. Technol.* **1989**, *7*, 1772.
- (23) Mitchell, J. A.; Reid, E. E. *J. Am. Chem. Soc.* **1931**, *53*, 1879.
- (24) Jursic, B. S.; Zdravkovski, Z. *Synth. Commun.* **1993**, *23*, 2761.
- (25) Goossen, L. J.; Ohlmann, D. M.; Lange, P. P. *Synthesis Stuttgart* **2009**, 160.
- (26) Dellinger, J. A.; Roberts, C. W. *Polym. Lett.* **1976**, *14*, 167.
- (27) Seijas, J. A.; Vazquez-Tato, M. P.; Montserrat-Martinez, M.; Nunez-Corredoira, G. *J. Chem. Res. (S)* **1999**, 420.
- (28) Sigel, H.; Martin, R. B. *Chem. Rev.* **1982**, *82*, 385.
- (29) Lodeiro, C.; Capelo, J. L.; Mejuto, J. C.; Oliveira, E.; Santos, H. M.; Pedras, B.; Nunez, C. *Chem. Soc. Rev.* **2010**, *39*, 2948.
- (30) Niyogi, S.; Bekyarova, E.; Itkis, M. E.; Zhang, H.; Shepperd, K.; Hicks, J.; Sprinkle, M.; Berger, C.; Lau, C. N.; de Heer, W. A.; Conrad, E. H.; Haddon, R. C. *Nano Lett.* **2010**, *10*, 4061.
- (31) Tuinstra, F.; Koenig, J. L. *Bull. Am. Phys. Soc.* **1970**, *15*, 296.
- (32) Eda, G.; Lin, Y.-Y.; Mattevi, C.; Yamaguchi, H.; Hsin-An Chen, H.-A.; Chen, I.-S.; Chen, C. W.; Chhowalla, M. *Adv. Mater.* **2010**, *22*, 505.
- (33) Loh, K. P.; Bao, Q. L.; Eda, G.; Chhowalla, M. *Nature Chem.* **2010**, *2*, 1015.
- (34) Kagan, M. R.; McCreery, R. L. *Anal. Chem.* **1994**, *66*, 4159.